

## The microRNA-455 null mouse shows dysregulated bone turnover

Lingzi Niu PhD<sup>1</sup>, Tracey E Swingler PhD<sup>1</sup>, Caterina Suelzu PhD<sup>2</sup>, Adel Ersek PhD<sup>2</sup>, Isabel R Orriss PhD<sup>3</sup>, Matthew J Barter PhD<sup>4</sup>, Dan J Hayman PhD<sup>4</sup>, David A Young PhD<sup>4</sup>, Nicole Horwood PhD<sup>2</sup>, Ian M Clark PhD<sup>1\*</sup>

<sup>1</sup>Biomedical Research Centre, School of Biological Sciences, University of East Anglia, Norfolk, UK.

<sup>2</sup> Norwich Medical School, University of East Anglia, UK

<sup>3</sup> Royal Veterinary College, London, UK

<sup>4</sup>Institute of Genetic Medicine, Newcastle University, Newcastle-upon-Tyne, UK.

\*Corresponding author:

Prof. Ian M. Clark,

Biomedical Research Centre, School of Biological Sciences,

Norwich Research Park, University of East Anglia,

Norwich, NR4 7TJ. UK.

Tel. +44(1603) 592760

Email: [i.clark@uea.ac.uk](mailto:i.clark@uea.ac.uk)

**Key words:** microRNA, miR-455, null mouse, bone, FGF18

**Data availability statement:** RNASeq data is available via the Gene Expression Omnibus (<https://www.ncbi.nlm.nih.gov/geo/>).

**Funding:** LN and TES were funded by a Dunhill Medical Trust Programme grant (number R476/0516).

**Ethical approval:** All experimental procedures and protocols used in this study were reviewed and approved by the Animal Welfare and Ethical Review Body (AWERB) and were conducted within the provisions of the U.K. Home Office Animals (Scientific Procedures) Act 1986 (PF50C7689)

**Conflicts of Interest:** The authors declare no conflict of interest.

**Acknowledgments:** We would like to thank staff in the Disease Modelling Unit for their generous help with these studies.

**Author contributions:** LN (investigation, formal analysis, writing), TES (investigation, reviewing and editing), CS (methodology, reviewing and editing), AE (methodology, reviewing and editing), IRO (methodology, reviewing and editing), MJB (methodology, reviewing and editing), DJH (methodology, reviewing and editing), DAY (conceptualization, supervision, funding acquisition, reviewing and editing), NH (conceptualization, supervision, methodology, reviewing and editing), IMC (conceptualization, funding acquisition, formal analysis, writing, reviewing and editing)

## **Abstract**

A wide range of specific microRNAs have been shown to have either positive or negative effects on osteoblast differentiation and function with consequent changes in post-natal bone mass; a number of specific targets have been identified. We previously used CrispR-Cas9 to make a miR-455 null mouse, characterising a behavioural phenotype with age. The current study identifies a bone phenotype, starting in younger animals.

At three weeks of age, the miR-455 null mice (both male and female) display increased length of both long bones and vertebrae and whilst this difference diminishes across 1 year, it remains significant. Increased bone formation in vivo is mirrored by an increase in osteogenesis from bone marrow-derived stem cells in vitro. This is accompanied by a decrease in osteoclastogenesis and osteoclast function. MicroCT analyses show increased trabecular bone and less porosity/decreased separation in the miR-455 null mouse suggesting a more dense and stronger bone at three weeks of age, these differences normalise by 1 year. Gain-of-function and loss-of-function datasets shows that *FGF18* expression is regulated by miR-455, and *FGF18* was validated as a direct target of miR-455. The regulation of *FGF18* by miR-455 is a likely mediator of its effect on bone.

## **Lay summary**

MicroRNAs are small molecules that have profound effects on the production of proteins and therefore on the function of cells and animal physiology. We made a mouse that lacks a specific microRNA, microRNA-455. This mouse has an increase in bone length from three-weeks of age. There is an increase in bone formation by bone forming cells (osteoblasts) and a decrease in bone loss (mediated by osteoclasts). Whilst several genes/proteins are altered by the absence of microRNA-455, a factor called fibroblast growth factor 18 (FGF18) is increased. This is likely to be a key mediator of the impact of microRNA-455 on bone.

## **Introduction**

The mutation or deletion of Dicer, an RNase, prevents the biogenesis of the majority of microRNAs, and studies on Dicer null mice demonstrated a strong role for microRNAs in skeletal development. Conditional knockout of Dicer in limb mesenchyme at the early stages of embryonic development leads to the formation of a smaller limb<sup>1</sup>. Dicer null growth plates show lack of chondrocyte proliferation, but also enhanced hypertrophy<sup>1</sup>. Conditional knockout of Dicer in chondrocytes results in skeletal growth defects and premature death<sup>2</sup>. Conditional Dicer knockout in osteoprogenitor cells or in osteoblasts themselves can lead to either a postnatal decrease or increase in bone depending on which cells are targeted and the timing of the deletion<sup>3-5</sup>. Deletion of Dicer in osteoclasts leads to an increase in postnatal bone mass<sup>6,7</sup>. A wide range of specific miRNAs have been shown to have either positive or negative effects on bone cell differentiation and function with consequent changes in post-natal bone mass, with a number of specific targets identified<sup>8</sup>.

MicroRNA-455 is genomically located in an intron of *COL27A1* which encodes collagen type XXVII. We discovered that miR-455 is co-regulated with miR-140 in both ATDC5 and human mesenchymal stem cell (hMSC) models of chondrogenesis<sup>9,10</sup> and is highly Sox9 inducible<sup>9</sup>. miR-455-3p has been shown to act in early chondrogenic differentiation via direct targeting of RUNX2<sup>11</sup> and potentially HDAC2 and HDAC8<sup>12</sup>. It may also impact on DNA methylation during chondrogenesis via DNMT3A<sup>13</sup>.

Two groups, as well as ours, have recently reported a miR-455 null mouse<sup>14-16</sup>. Ito et al. found no differences in skeletal formation at P2 on skeletal prep, with microCT analysis at 8 weeks old showing no significant difference in bone volume, bone mineral density and microarchitecture of the femur<sup>15</sup>. Articular cartilage degeneration was not seen at 2 months of age but was apparent at 6 months with an increase in catabolic gene expression. HIF-2a was identified as a direct target of miR-455 which mediated the cartilage phenotype<sup>15</sup>. Hu et al. reported a miR-455 null mouse but with little detail given, however, cartilage thickness was decreased in 6 month old mice<sup>14</sup>. In Mao et al, the same mouse showed similar cartilage loss at 10 months of age<sup>16</sup>.

We reported our miR-455 null mouse showing a behavioural phenotype at 14 months of age, with significant recognition memory deficit and a slight increase in anxiety<sup>17</sup>. A similar cognitive phenotype in a miR-455 null mouse was described by Kumar et al (2021), with the converse shown in a transgenic mouse overexpressing miR-455-3p<sup>18</sup>. MicroRNA-455 null mice also showed decreased lifespan, again

with the converse shown in the transgenic line<sup>18</sup>. These phenotypes were associated with mitochondrial function<sup>18,19</sup>.

Here, we report a bone phenotype in our miR-455 null strain with a significant difference in both femur and vertebral length at 3 weeks of age. Bone formation in the null mice increased *in vivo*, whilst osteogenesis from bone marrow-derived mesenchymal stem cells increased *in vitro*. MicroRNA-455 nulls cells also showed decreased osteoclastogenesis and osteoclast function.

## **Materials and Methods**

### MicroRNA-455 null mouse

MicroRNA-455 null mice were made using CrispR-Cas9 by the Transgenic Unit, University of Manchester (<https://sites.manchester.ac.uk/genome-editing-unit>) and bred to the C57/BL6 background as described<sup>17</sup>. A 35-base deletion (confirmed by sequencing) removes part of both miR-455-3p and miR-455-5p along with the intervening hairpin. MicroRNA-455 was not expressed in the null in any tissue tested whilst expression of *Col27a1* was unaffected. All mouse experiments were performed in compliance with the ARRIVE guidelines (<https://www.nc3rs.org.uk/arrive-guidelines>) under license (PF50C7689) granted from the Home Office (United Kingdom) in accordance with the guidelines and regulations for the care and use of laboratory animals outlined by the Animals (Scientific Procedures) Act 1986 according to Directive 2010/63/EU of the European Parliament. Protocols were approved by the Animal Ethics Committee of the University of East Anglia and the Home Office, United Kingdom.

### Measurement of bone length

Mouse tails and hind limbs were harvested at 3 weeks, 6 months and 1 year, followed by fixation in 10% (w/v) neutral-buffered formalin (NBF, Sigma-Aldrich, Merck) for 24 hours at room temperature and storage in 70% (v/v) ethanol at 4 °C until scanned. Plain X-ray imaging was conducted using the Bruker In-Vivo Xtreme system (Bruker). Maximal axial length of caudal vertebrae and limb bones was measured using Fiji Image J. The femur length was defined by the distance between most proximal/superior point of the femur head and the most distal point of the femoral condyle along the long axis. The tibia length was defined by the maximal distance between the medial tibial plateau and the tibial plafond along the long axis.

### MicroCT

Mouse hind limbs were dissected, fixed and dehydrated as mentioned above. After rehydration in PBS for 30 minutes, tibiae were scanned using a Skyscan 1174 (Bruker) with 0.5 mm aluminium filter, and

settings of 50 kV, 800 mA, 8.28  $\mu\text{m}$  camera pixels, 0.7 ° rotation step and 2 frames averaging. Initial scans of trabecular and cortical bones were reconstructed using NRecon (Bruker) and analysed with CTAn (Bruker) according to the manufacturer. A volume of interest (VOI) encompassing the 1.2 mm region distal to the growth plate were selected for trabecular bone, while a VOI of a further 0.6 mm were applied for cortical bone. 3D visualization of the tibiae was generated using Ctvol (Bruker).

#### Calcein incorporation

Calcein green (Sigma-Aldrich, Merck) was intraperitoneally injected into mice at 20 mg/kg at 1 and 3 days after weaning at P21. Tibiae were dissected 2 days after final injection (P26), fixed with 10% (w/v) NBF, dehydrated in gradient ethanol and embedded in methyl methacrylate. Embedded tibiae were sectioned longitudinally and imaged using fluorescence microscopy (DMI3000B, Leica) equipped with megapixel digital colour camera (DFC310 FX, Leica). Mineral apposition rate (MAR) was calculated based on the average distance of 2 calcein-labelled layers of the cortical bone per day.

#### Osteogenesis

Murine bone marrow stromal cells were isolated from the long limb bones of 3-4 week old mice and subcultured in DMEM supplemented with 10% (v/v) FBS and 1% (v/v) Penicillin/Streptomycin (all from Gibco, Thermo Fisher Scientific), adapted from the method described<sup>20</sup>. Murine BMSCs at passage 3 were seeded in 48-well plate at a density of  $6 \times 10^5$  cells/well for Alizarin Red S staining, and in 96-well plate at  $1.5 \times 10^5$  cells/well for qRT-PCR and alkaline phosphate assay (ALP assay). Experiments were performed in quadruplicate for each mouse. Osteogenesis was induced by osteogenic medium consisting of 100 nM dexamethasone (Sigma-Aldrich, Merck), 10 mM  $\beta$ -glycerol phosphate (Sigma-Aldrich, Merck), 50  $\mu\text{g}/\text{mL}$  ascorbic acid 2-phosphate (Sigma-Aldrich, Merck), 10% (v/v) FBS and 1% (v/v) Pen/Strep in high-glucose DMEM (Gibco, Thermo Fisher Scientific). Osteogenic medium was changed every 3 days until desired time points.

#### Alizarin Red S staining

Alizarin Red S staining was performed for analyzing calcium deposition of murine BMSCs undergoing osteogenesis for 28 days. Staining and quantification methods were adapted from<sup>21</sup>. Briefly, cells were washed with PBS and fixed in 4% (w/v) formaldehyde (Sigma-Aldrich, Merck) for 1 hour at room temperature. Fixed cells were then immersed in 40 mM Alizarin Red S solution (Sigma-Aldrich, Merck) for 30 minutes, washed in double-distilled H<sub>2</sub>O and air dried. 10% (w/v) cetylpyridinium chloride was used to dissolve Alizarin Red S. Eluents were transferred into a 96-well plate. Absorbance was measured at 595nm using the EnVision 2103 plate reader (PerkinElmer).

#### Alkaline phosphate assay

Colorimetric alkaline phosphate (ALP) assay was conducted to measure ALP activity of osteogenic murine BMSCs. Cells were washed with PBS, followed by adding 20  $\mu$ L double-distilled H<sub>2</sub>O and 100  $\mu$ L alkaline phosphatase yellow (pNPP) liquid substrate system (Sigma-Aldrich, Merck). Plates were then incubated at 37 °C for 20 minutes. 80  $\mu$ L of stop solution composed of 0.2 M NaOH was added and mixed thoroughly. Absorbance was detected at 405 nm. The concentration of ALP was calculated regarding to a standard curve generated from a series of ALP solutions of known concentrations.

### Osteoclastogenesis

Isolation and culture for murine osteoclasts on dentine were carried out using adapted published methods<sup>22,23</sup>. Non-adhesive bone marrow cells were collected and seeded at  $1 \times 10^5$  cells/well on sterile dentine discs in 96-well plates. Experiments were performed in quadruplicate for each mouse. Seeded cells were cultured in  $\alpha$ MEM (Gibco, Thermo Fisher Scientific) containing 10% (v/v) FBS (Gibco, Thermo Fisher Scientific), 1% (v/v) Pen/Strep (Gibco, Thermo Fisher Scientific), 100 ng/mL recombinant mouse M-CSF (R&D Systems, Bio-Techne) for 2 days. Medium was subsequently changed to  $\alpha$ MEM supplemented with 10% (v/v) FBS (Gibco, Thermo Fisher Scientific), 1% (v/v) Pen/Strep (Gibco, Thermo Fisher Scientific), 20 ng/mL recombinant mouse M-CSF (R&D Systems, Bio-Techne) and 50 ng/mL recombinant mouse Rank Ligand (R&D Systems, Bio-Techne) for 4 days.  $\alpha$ MEM was then acidified by adding concentrated HCl to get a final concentration of 0.01 N. Cells were further incubated in the acidified  $\alpha$ MEM for 3 days to achieve a basal level of resorption.

### Tartrate resistant acid phosphatase (TRAP) assay

Cells were fixed using 10% (w/v) NBF for 1 hour and TRAP activity were measured using TRAP solution containing 0.2 mg/mL naphthol AS-MX phosphate, 1% (v/v) N,N-dimethylformamide and 0.4mg/mL fast red violet LB salt, for TRAP activity as described<sup>24</sup> (all from Sigma-Aldrich, Merck). Osteoclasts, defined as TRAP-positive cells with 3 or more nuclei, were examined using Fiji Image J. For histologic assessment, mouse knee joints were fixed in 10% (w/v) NBF, decalcified in 14% (w/v) EDTA, and eventually embedded in paraffin (all from Sigma-Aldrich, Merck). Frontal sections with 5 $\mu$ M thickness were serially cut using microtome (HM355S, Microm). Sections were stained with TRAP solution described above and counterstained with 0.06% (w/v) Fast Green (Sigma-Aldrich, Merck). A TrapHisto program<sup>25</sup> was applied for semi-automated quantification of osteoclasts in the primary spongiosa of tibiae.

### Resorption pits quantification

Cells were removed from the dentine discs in 1 M ammonium hydroxide (Sigma-Aldrich, Merck). Dentine discs were then stained in 0.5% (w/v) toluidine solution (Sigma-Aldrich, Merck) as described

by <sup>26</sup>. At least 3 independent views were imaged and examined for each disc. Surface area of pits was measured using Fiji Image J.

### Cell lines

Osteosarcoma cells 143B were a kind gift of Dr Darrell Green, UEA. DF1 is a spontaneously immortalized chicken dermal fibroblast cell line, a kind gift from Prof. Andrea Munsterberg, UEA. The chondrosarcoma cell line SW1353 was derived from human chondrosarcoma of humerus and purchased from ATCC. Cells were cultured in DMEM supplemented with 10% (v/v) FBS and 1% (v/v) Pen/Strep (Gibco, Thermo Fisher Scientific) at 37 °C incubator with 5% (v/v) CO<sub>2</sub>.

### Target identification

Three RNASeq datasets were used for target identification described in <sup>27</sup>. These were from (i) knee cartilage from wild-type vs miR-455 null mice at age 3 months (GSE274395); (ii) SW1353 cells transfected with mimics or inhibitors of miR-455-3p vs negative controls (as described above, GSE276347); (iii) chick limb bud microinjected with miR-455-3p mimic vs control (GSE276509). Differentially expressed genes were ranked based on fold change and q-values.

### Transient transfection and target validation

143B human osteosarcoma cells were seeded in 96-well plates at a density of  $7 \times 10^3$  cells/well. The next day, cells were transfected with 150 nM miR-455-3p mimic (hsa-miR-455-3p miRCURY LNA miRNA Mimic, Qiagen) vs a non-targeting negative control (Negative Control miRCURY LNA miRNA Mimic, Qiagen) using Lipofectamine 2000 (Thermo Fisher Scientific). For transfection of miR-455-3p inhibitor (hsa-miR-455-3p miRCURY LNA miRNA Inhibitor, Qiagen) or inhibitor control (Negative control A miRCURY LNA miRNA Inhibitor Control, Qiagen), a final concentration of 75 nM were used. All microRNA mimics, inhibitors and controls were from Qiagen. Transfected cells were further incubated for 48 hours and harvested for qRT-PCR as previously described <sup>28</sup>. Cells were lysed and total RNAs were reverse-transcribed using Cell-to-cDNA II kit (Ambion, Thermo Fisher Scientific), followed by real-time PCR performed with PCR 7500 system (Applied Biosystems). Primers (Sigma-Aldrich, Merck) and Universal Probe Library IDs (Roche) are listed in Supplementary Table 1.

For luciferase assays, 3'UTR luciferase reporters were constructed using the In-Fusion HD Cloning kit (TaKaRa Bio), where the 3'UTR of human mRNAs predicted to be targets of miR-455 were inserted downstream of the firefly luciferase reporter of the pmirGLO Dual-Luciferase miRNA target expression vector (Promega). Non-functional mutations were introduced to the miR-455 seed sites using QuikChange II XL site-directed mutagenesis (Agilent). DF1 cells were transfected with 50 nM miR-455-3p mimic or non-targeting control (as above) using Lipofectamine 2000; 24 hours after

miRNA transfection, cells were transfected with 100 ng 3'UTR luciferase reporters, and incubated for a further 48 hours. Firefly and Renilla luminescence were quantified using the Dual-Glo luciferase assay system (Promega) and a multilabel plate reader (EnVision 2103, PerkinElmer). Primers (Sigma-Aldrich, Merck) for subcloning and mutagenesis are listed in Supplementary Table 2.

### Statistical analysis

Data were tested for normal distribution comparison between two means analysed using Student's t-test. One-way ANOVA with post-hoc Tukey's test was used to compare between multiple samples using GraphPad Prism version 9.

## **Results**

### MicroRNA-455 null mice have increased bone length

We have previously shown that miR-455 null mice were significantly heavier than wild-type from around 6 months of age<sup>17</sup>. The length of the caudal vertebrae (from Ca4 to Ca16) were measured by X-ray at 3 weeks of age (Figure 1A) with those from miR-455 null mice showing greater length (of Ca12 to Ca16) than wild-type. More distal caudal vertebrae showed a greater increase in length compared to the proximal vertebrae, with a similar pattern displayed at 6 months of age (data not shown). Femur and tibia length were measured using X-ray at 3 weeks, 6 months and 12 months of age. Femur length was significantly more in miR-455 null mice at all ages, though in tibia, it only remained significant at 3 weeks of age (Figure 1B, C). Whilst Figure 1 analyses both sexes of mice, these are plotted separately in Supplementary Figure 1, showing identical patterns. Measurement of the growth plate at 3 weeks of age showed a small statistically increase in overall size in miR-455 null vs wild-type, coming from an increase in the size of the resting zone and a decrease in the hypertrophic zone in the miR-455 null mice (both  $p < 0.05$ , Supplementary Figure 2).

### MicroRNA-455 null mice exhibit greater bone deposition and osteogenesis

Bone formation in the mouse femur was assessed by double calcein labelling. Quantification of matrix apposition rate shows significantly increased bone formation in the miR-455 null mice compared to wild-type (Figure 2A, B), demonstrating increased osteoblast function. Bone marrow-derived stem cells were extracted from the long bones of mice at P21 and differentiated into mature osteoblasts over 28 days. Alizarin Red staining demonstrating increased bone formation, with alkaline phosphatase activity in the medium increasing from day 7 (Figure 2 C,D). Alkaline phosphatase staining increases in the miR-455 null mice compared to wild-type from day 7 onwards (Figure 2E). BMSC were also differentiated through adipogenesis across 14 days and although Oil Red O staining was greater in wild-type compared to miR-455 null mice, there was substantial cell

death and the number of remaining adipocytes was low (data not shown). In order to support this, adipocyte ghosts were stained in the bone marrow of 3 week old mice, showing that the number of adipocyte ghosts was decreased in the miR-455 null mice (Supplementary Figure 3).

#### MicroRNA-455 null mice exhibit decreased osteoclastogenesis

MCSF-dependent bone marrow macrophages were cultured from the bone marrow of 3 week old miR-455 null or wild-type mice and subjected to an osteoclastogenesis assay with cells cultured on dentine slices. TRAP staining identified a significant increase in multinucleated osteoclasts in wild-type cells compared to miR-455 null (Figure 3A, B), whilst Toluidine Blue staining showed a significant increase in bone resorption too (Figure 3C, D). This indicates that miR-455 knockout leads to decreased differentiation to osteoclasts, along with a potential decrease in function.

In vivo, TRAP staining in 3 week old mice showed a significant decrease in TRAP-positive osteoclasts per unit area in the miR-455 null mice compared to wild-type. However, this difference is not apparent after normalisation to bone volume (Figure 3E, F).

#### MicroRNA-455 null mice show changes in both trabecular and cortical bone

MicroCT analysis shows that trabecular volume, as a percentage of total volume, increases in the miR-455 null mouse at 3 weeks old in both male and females (Figure 4A). Both trabecular number and thickness also increase in the miR-455 null at this age (Figure 4B, C). There is a decrease in trabecular separation and therefore a decrease in porosity (Figure 4D) in the miR-455 null too. All of the changes lose significance at 1 year of age and there is no difference between males and females of different genotypes (plotted together). These changes are mirrored for cortical bone (Supplementary Figure 4). A reconstruction of bone features is shown in Figure 4E.

#### *FGF18* is a direct target for microRNA-455

We had available a number of RNA-Seq datasets in which we explored the expression of genes relevant to the skeleton (see Methods, though these were not datasets from bone or bone cells). Table 1 shows 12 genes which were increased in expression >2-fold ( $p < 0.05$ ) within articular cartilage taken from 3 month-old miR-455 null mice compared to wild-type with the addition of *Bmpr1a* which has 9 predicted seed sites for miR-455-3p in its 3'UTR. We compared this to the expression in SW1353 cells overexpressing either miR-455-3p mimic or inhibitor and also chick limb bud microinjected with miR-455-3p mimic. The only gene, following the expected expression pattern (increased in miR-455 null, decreased by miR-455-3p mimic and increased by miR-455 inhibitor) was *FGF18* which is also predicted to be a direct target for miR-455-3p. *BMP4* and *BMPRIA* were also pursued, though *BMP4* has no seed sites for miR-455-3p in its 3'UTR. In 143B human osteosarcoma cells, *FGF18* and

*BMP4* expression was decreased by overexpression of miR-455-3p mimic and increased by overexpression of miR-455-3p inhibitor (Figure 5A-C). No effect was seen on the expression of *BMPRIA*. The 3'UTR of the *FGF18* and *BMP4* gene were subcloned into pmIR-GLO (wild-type) and the seed site(s) for miR-455-3p mutated (mutant), constructs were transiently transfected into chicken DF1 fibroblasts in the presence of either a control miR mimic or miR-455-3p mimic. Luciferase assays (Figure 5D-E) show that the 3'UTR of both genes is repressed by miR-455-3p mimic but only *FGF18* is rescued by mutation of the seed site, implying that *FGF18* is a direct target for miR-455-3p, but *BMP4* is not.

### **Discussion:**

The most detailed previous analysis of a miR-455 null mouse was performed by Ito et al.<sup>15</sup>. The authors did not show any difference in bone morphometry either postnatally or at 8 weeks of age. Though their microCT analyses used only groups of n=3 male mice, our data show that there would likely be a measurable difference in bone, even at that group size. Differences in the resolution of the microCT system used may also have an impact on measurement here. Ito et al. also showed a difference in spontaneous cartilage destruction with age, apparent at 6 months. Our analyses of cartilage do not show such a difference out to 1 year of age (data not shown). However, in a pilot (n=6) experiment of the DMM model, we did see a statistically significant (p<0.05) increase in OARSI score in the miR-455 null mice compared to wild-type when all joint compartments were summed (Supplementary Figure 5). We have reported the same behavioural phenotype in our miR-455 null mice to Kumar et al.<sup>18</sup>.

In agreement with the literature, there is no significant difference in bone length between males and females within either genotype<sup>29</sup>. The increase in long bone length measured in the miR-455 null vs. wild-type mice is most apparent at 3 weeks of age, diminishing with age. At this early time point, there was a significant difference in growth plate height, but it is unclear if this is sufficient to explain changes in downstream bone length. However, this growth plate difference came from an increase in resting zone height and a previous detailed morphometric analysis showed that this correlated with bone length and bone growth rate in mice, whereas hypertrophic zone height did not<sup>30</sup>.

Both in vivo and in vitro, the miR-455 null mouse or cells derived from it, showed effects on both bone formation (osteoblasts) and resorption (osteoclasts), with increased bone formation and decreased bone resorption in the miR-455 null. Data gained using cells from young (3 week old) animals is consistent with the microCT data.

In microCT analyses, increased trabecular bone and less porosity/decreased separation would suggest a more dense and stronger bone, though this wasn't tested functionally. The difference between miR-455 null mice and wild-type in measures of microCT disappears by 1 year of age despite the difference in long bone length remaining (though decreased). Interestingly, we have previously reported decreased expression of miR-455 in wild-type mice across age <sup>17</sup>.

In order to understand the molecular function of miR-455 in driving the bone phenotype, we made use of existing gene expression datasets in previous studies of cartilage, using tissue or cell models of genetic deletion of miR-455 or forced overexpression of inhibition. These were accessible data sets, rather than studies in the bone cells that would be more appropriate to the research question.

Comparison of these datasets and analysis of potential miR-455 target sites in the 3'UTR of resultant genes, led us to investigate *FGF18*, *BMP4* and *BMP1RA* further. In a human osteosarcoma cell line, expression of *FGF18* and *BMP4* followed the same pattern as in the RNA-Seq data from SW1353 chondrosarcoma cells. Luciferase assays showed *FGF18* as a direct target of miR-455-3p, however the repression of luciferase expression driven by the *BMP4* 3'UTR was not rescued by ablation of the miR-455 seed site. Either this gene is not a direct target for miR-455-3p, or further, cryptic miR-455 seed sites remain in the 3'UTR. *Fgf18* has previously been shown to be required for osteogenesis in the mouse embryo <sup>31</sup>, whilst the growth plate of the *Fgf18* null mouse is also elongated <sup>32</sup>.

Interestingly, overexpression or addition of *Fgf18* enhances osteogenesis from C3H10T1/2 cells <sup>33</sup>. Osteoclasts do not express *FGF18*, though they may respond to it <sup>34</sup>, however, the mechanism of action of miR-455 in osteoclasts requires further work. Whilst any microRNA likely has multiple gene targets that bring about functional effect, *FGF18* is clearly a prime candidate to mediate the function of miR-455 on bone.

In summary, the miR-455 null mouse displays a bone phenotype, underpinned by effects on both bone formation and resorption. *FGF18* has been identified as a direct target for miR-455-3p which may mediate this effect. Further research is needed to understand further the detail of molecular pathways involved.

## **References**

1. Harfe BD, McManus MT, Mansfield JH, Hornstein E, Tabin CJ. The RNaseIII enzyme Dicer is required for morphogenesis but not patterning of the vertebrate limb. *Proc Natl Acad Sci U S A*. Aug 2 2005;102(31):10898-903. doi:10.1073/pnas.0504834102
2. Kobayashi T, Lu J, Cobb BS, et al. Dicer-dependent pathways regulate chondrocyte proliferation and differentiation. *Proc Natl Acad Sci U S A*. Feb 12 2008;105(6):1949-54. doi:10.1073/pnas.0707900105
3. Bendre A, Moritz N, Vaananen V, Maatta JA. Dicer1 ablation in osterix positive bone forming cells affects cortical bone homeostasis. *Bone*. Jan 2018;106:139-147. doi:10.1016/j.bone.2017.10.018

4. Gaur T, Hussain S, Mudhasani R, et al. Dicer inactivation in osteoprogenitor cells compromises fetal survival and bone formation, while excision in differentiated osteoblasts increases bone mass in the adult mouse. *Dev Biol.* Apr 1 2010;340(1):10-21. doi:10.1016/j.ydbio.2010.01.008
5. Liu P, Baumgart M, Groth M, et al. Dicer ablation in osteoblasts by Runx2 driven cre-loxP recombination affects bone integrity, but not glucocorticoid-induced suppression of bone formation. *Sci Rep.* Aug 24 2016;6:32112. doi:10.1038/srep32112
6. Mizoguchi F, Izu Y, Hayata T, et al. Osteoclast-specific Dicer gene deficiency suppresses osteoclastic bone resorption. *J Cell Biochem.* Apr 1 2010;109(5):866-75. doi:10.1002/jcb.22228
7. Sugatani T, Hruska KA. Impaired micro-RNA pathways diminish osteoclast differentiation and function. *J Biol Chem.* Feb 13 2009;284(7):4667-78. doi:10.1074/jbc.M805777200
8. Hensley AP, McAlinden A. The role of microRNAs in bone development. *Bone.* Feb 2021;143:115760. doi:10.1016/j.bone.2020.115760
9. Barter MJ, Tselepi M, Gomez R, et al. Genome-Wide MicroRNA and Gene Analysis of Mesenchymal Stem Cell Chondrogenesis Identifies an Essential Role and Multiple Targets for miR-140-5p. *Stem Cells.* Nov 2015;33(11):3266-80. doi:10.1002/stem.2093
10. Swingler TE, Wheeler G, Carmont V, et al. The expression and function of microRNAs in chondrogenesis and osteoarthritis. *Arthritis Rheum.* Jun 2012;64(6):1909-19. doi:10.1002/art.34314
11. Zhang Z, Hou C, Meng F, et al. MiR-455-3p regulates early chondrogenic differentiation via inhibiting Runx2. *FEBS Lett.* Nov 30 2015;589(23):3671-8. doi:10.1016/j.febslet.2015.09.032
12. Chen W, Chen L, Zhang Z, et al. MicroRNA-455-3p modulates cartilage development and degeneration through modification of histone H3 acetylation. *Biochim Biophys Acta.* Dec 2016;1863(12):2881-2891. doi:10.1016/j.bbamcr.2016.09.010
13. Sun H, Zhao X, Zhang C, et al. MiR-455-3p inhibits the degenerate process of chondrogenic differentiation through modification of DNA methylation. *Cell Death Dis.* May 1 2018;9(5):537. doi:10.1038/s41419-018-0565-2
14. Hu S, Zhao X, Mao G, et al. MicroRNA-455-3p promotes TGF-beta signaling and inhibits osteoarthritis development by directly targeting PAK2. *Exp Mol Med.* Oct 4 2019;51(10):1-13. doi:10.1038/s12276-019-0322-3
15. Ito Y, Matsuzaki T, Ayabe F, et al. Both microRNA-455-5p and -3p repress hypoxia-inducible factor-2alpha expression and coordinately regulate cartilage homeostasis. *Nat Commun.* Jul 6 2021;12(1):4148. doi:10.1038/s41467-021-24460-7
16. Mao G, Kang Y, Lin R, et al. Long Non-coding RNA HOTTIP Promotes CCL3 Expression and Induces Cartilage Degradation by Sponging miR-455-3p. *Front Cell Dev Biol.* 2019;7:161. doi:10.3389/fcell.2019.00161
17. Swingler TE, Niu L, Pontifex MG, Vauzour D, Clark IM. The microRNA-455 Null Mouse Has Memory Deficit and Increased Anxiety, Targeting Key Genes Involved in Alzheimer's Disease. *Int J Mol Sci.* Jan 5 2022;23(1)doi:10.3390/ijms23010554
18. Kumar S, Morton H, Sawant N, et al. MicroRNA-455-3p improves synaptic, cognitive functions and extends lifespan: Relevance to Alzheimer's disease. *Redox Biol.* Nov 9 2021;48:102182. doi:10.1016/j.redox.2021.102182
19. Kumar S, Reddy AP, Yin X, Reddy PH. Novel MicroRNA-455-3p and its protective effects against abnormal APP processing and amyloid beta toxicity in Alzheimer's disease. *Biochim Biophys Acta Mol Basis Dis.* Sep 1 2019;1865(9):2428-2440. doi:10.1016/j.bbadis.2019.06.006
20. Huang S, Xu L, Sun Y, Wu T, Wang K, Li G. An improved protocol for isolation and culture of mesenchymal stem cells from mouse bone marrow. *J Orthop Translat.* Jan 2015;3(1):26-33. doi:10.1016/j.jot.2014.07.005
21. Johnson de Sousa Brito FM, Butcher A, Pisconti A, et al. Syndecan-3 enhances anabolic bone formation through WNT signaling. *FASEB J.* Apr 2021;35(4):e21246. doi:10.1096/fj.202002024R
22. Orriss IR, Arnett TR. Rodent osteoclast cultures. *Methods Mol Biol.* 2012;816:103-17. doi:10.1007/978-1-61779-415-5\_8
23. Cohen-Karlik E, Awida Z, Bergman A, et al. Quantification of Osteoclasts in Culture, Powered by Machine Learning. *Front Cell Dev Biol.* 2021;9:674710. doi:10.3389/fcell.2021.674710

24. Ersek A, Santo AI, Vattakuzhi Y, George S, Clark AR, Horwood NJ. Strain dependent differences in glucocorticoid-induced bone loss between C57BL/6J and CD-1 mice. *Sci Rep*. Nov 4 2016;6:36513. doi:10.1038/srep36513
25. van 't Hof RJ, Rose L, Bassonga E, Daroszewska A. Open source software for semi-automated histomorphometry of bone resorption and formation parameters. *Bone*. Jun 2017;99:69-79. doi:10.1016/j.bone.2017.03.051
26. Danks L, Workman S, Webster D, Horwood NJ. Elevated cytokine production restores bone resorption by human Btk-deficient osteoclasts. *J Bone Miner Res*. Jan 2011;26(1):182-92. doi:10.1002/jbmr.210
27. Paddy P. *MicroRNA-455 in cartilage and skeletal development*. University of East Anglia; 2021. <https://ueaeprints.uea.ac.uk/id/eprint/87538>
28. Le L, Niu L, Barter MJ, et al. The role of microRNA-3085 in chondrocyte function. *Sci Rep*. Dec 14 2020;10(1):21923. doi:10.1038/s41598-020-78606-6
29. Somerville JM, Aspden RM, Armour KE, Armour KJ, Reid DM. Growth of C57BL/6 mice and the material and mechanical properties of cortical bone from the tibia. *Calcif Tissue Int*. May 2004;74(5):469-75. doi:10.1007/s00223-003-0101-x
30. Wilson K, Usami Y, Hogarth D, et al. Analysis of Association between Morphometric Parameters of Growth Plate and Bone Growth of Tibia in Mice and Humans. *Cartilage*. Dec 2021;13(2\_suppl):315S-325S. doi:10.1177/1947603519900800
31. Ohbayashi N, Shibayama M, Kurotaki Y, et al. FGF18 is required for normal cell proliferation and differentiation during osteogenesis and chondrogenesis. *Genes Dev*. Apr 1 2002;16(7):870-9. doi:10.1101/gad.965702
32. Liu Z, Xu J, Colvin JS, Ornitz DM. Coordination of chondrogenesis and osteogenesis by fibroblast growth factor 18. *Genes Dev*. Apr 1 2002;16(7):859-69. doi:10.1101/gad.965602
33. Hamidouche Z, Fromigue O, Nuber U, et al. Autocrine fibroblast growth factor 18 mediates dexamethasone-induced osteogenic differentiation of murine mesenchymal stem cells. *J Cell Physiol*. Aug 2010;224(2):509-15. doi:10.1002/jcp.22152
34. Shimoaka T, Ogasawara T, Yonamine A, et al. Regulation of osteoblast, chondrocyte, and osteoclast functions by fibroblast growth factor (FGF)-18 in comparison with FGF-2 and FGF-10. *J Biol Chem*. Mar 1 2002;277(9):7493-500. doi:10.1074/jbc.M108653200

### **Figure legends:**

**Figure 1: Measurement of bone length across age.** A: Caudal (Ca) vertebrae were measured on X-ray and numbered from Ca4 (after lumbar vertebrae), n=4, t-test with Benjamini-Hochberg correction, \*,  $q < 0.05$ ; \*\*,  $q < 0.01$ ., mean +/- SEM. B, C: Length of tibia and femur were measured on X-ray, n=12-20, t-test with Benjamini-Hochberg correction, \*,  $q < 0.05$ ; \*\*,  $q < 0.01$ ; \*\*\*,  $q < 0.001$ .

**Figure 2: Osteoblast function and osteogenesis.** A, B. Sequential intraperitoneal calcein injections were undertaken were undertaken 2 days apart with sacrifice 48 hours later. Bone was embedded in methyl methacrylate, sections visualised and the amount of bone formed between the two injections quantified using image analysis, n=5, mean +/- SEM, Student's t-test, \*,  $p < 0.05$ . C. bone marrow-derived stem cells were differentiated through osteogenesis across 28 days and calcium phosphate stained using Alizarin Red, extracted and quantified in D. (n=6, 3 male (M) and 3 female (F), mean +/- 95% CI, Student's t-test, \*,  $p < 0.05$ ). E. Alkaline phosphatase in the conditioned medium was quantified (n=8, 4 male and 4 female, mean +/- 95% CI, 2 way ANOVA with Fisher's LSD \*,  $p < 0.05$ ).

**Figure 3: Osteoclastogenesis, osteoclast number and function.** A, B.: MCSF-dependent bone marrow macrophages were cultured from the bone marrow of 3-5 weeks old miR-455 null (KO) or wild-type (WT) mice and subjected to an osteoclastogenesis assay with cells cultured on dentine slices. TRAP staining identified and image analysis measured multinucleated osteoclasts (A, B), whilst Toluidine Blue (C, D) staining of dentine showed resorption pits. Mean +/- SEM, n=5, Student's t-test, \*,  $p < 0.5$ , \*\*,  $p < 0.01$ . TRAP staining in the distal tibia of 3 week old mice showed osteoclasts in the primary spongiosa (E), with quantification expressed per unit area (F) or bone volume (G). Scale bar = 100µm.

**Figure 4: MicroCT analysis of miR-455 null mouse vs. wild-type bone.** Mouse hind limbs were dissected, fixed and dehydrated and scanned using a Skyscan 1174 (Bruker), see Methods. A-D: Tb.BV/TV%, percent trabecular bone volume; Tb.N, trabecular number; Tb.Th, trabecular thickness; Tb.Sp, trabecular separation. E, Three dimensional visualization of the tibiae was generated using Ctvol (Bruker).

**Figure 5: Identification and validation of relevant miR-455 targets.** A: Human 143B osteosarcoma cells were transfected with 150 nM miR-455-3p mimic vs control or 75 nM miR-455-3p inhibitor vs control for 48 hr prior to measurement of gene expression by qRT-PCR. Results are expressed as fold expression compared to control (dotted line). B: Chick DF1 fibroblasts were transfected with 100 ng 3'UTR of FGF18 or BMP4 in pmiRGLO, either WT sequence or with miR-455-3p targets mutated (mutant) in the presence 50 nM miR-455-3p mimic or non-targeting control for 48 hrs prior to harvest and luciferase assay. Results are plotted relative to non-targeting control (dotted line). Mean +/- SEM, n=4, Student's t-test, \*, p<0.5, \*\*, p<0.01, \*\*\*, p<0.001.

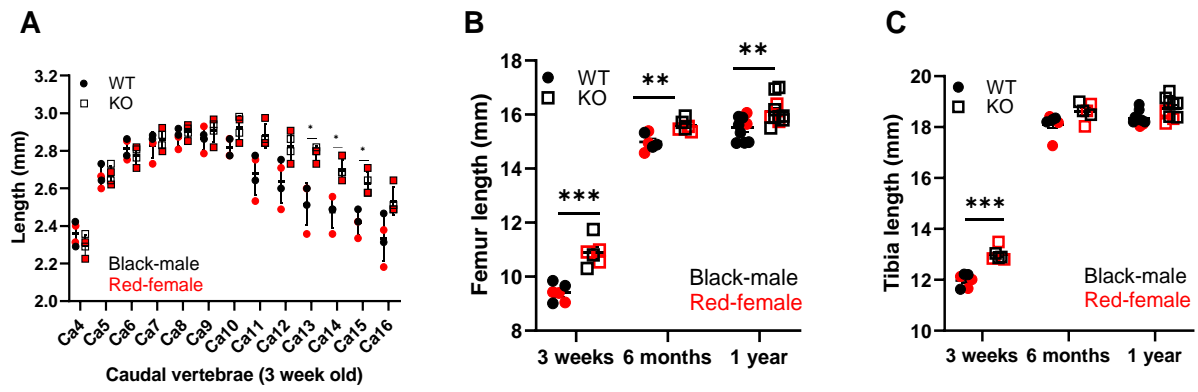


Figure 1: Measurement of bone length across age A: Caudal (Ca) vertebrae were measured on X-ray and numbered from Ca4 (after lumbar vertebrae),  $n=4$ , t-test with Benjamini-Hochberg correction, \*,  $q<0.05$ ; \*\*,  $q<0.01$ ., mean  $\pm$  SEM. B, C: Length of tibia and femur were measured on X-ray,  $n=12-20$ , t-test with Benjamini-Hochberg correction, \*,  $q<0.05$ ; \*\*,  $q<0.01$ ; \*\*\*,  $q<0.001$ .

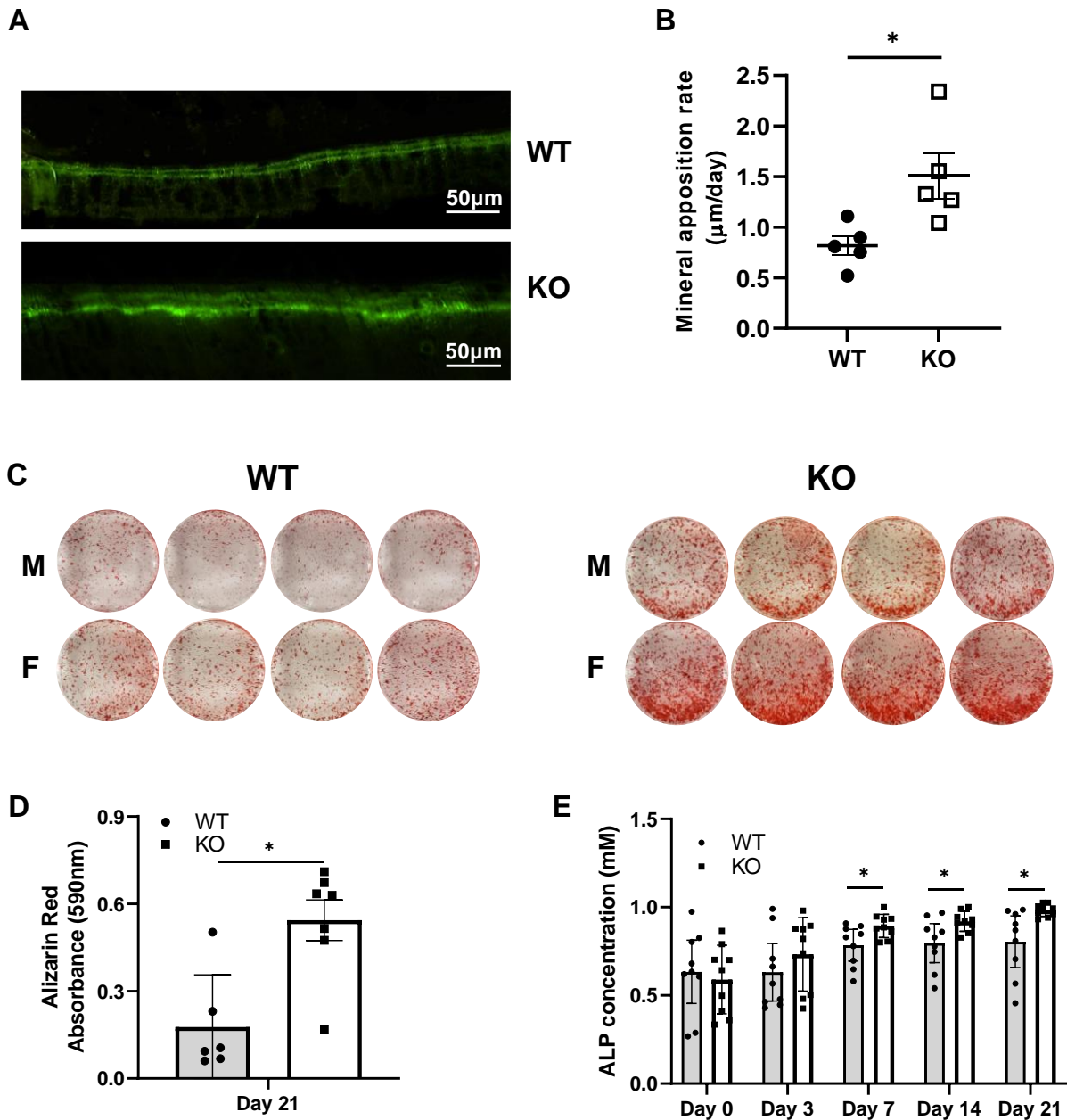


Figure 2: Osteoblast function and osteogenesis. A, B. Sequential intraperitoneal calcein injections were undertaken 2 days apart with sacrifice 48 hours later. Bone was embedded in methyl methacrylate, sections visualised and the amount of bone formed between the two injections quantified using image analysis,  $n=5$ , mean  $\pm$  SEM, Student's t-test, \*,  $p<0.05$ . C. bone marrow-derived stem cells were differentiated through osteogenesis across 28 days and calcium phosphate stained using Alizarin Red, extracted and quantified in D. ( $n=6$ , 3 male (M) and 3 female (F), mean  $\pm$  95% CI, Student's t-test, \*,  $p<0.05$ ). E. Alkaline phosphatase in the conditioned medium was quantified ( $n=8$ , 4 male and 4 female, mean  $\pm$  95% CI, 2 way ANOVA with Fisher's LSD \*,  $p<0.05$ ).

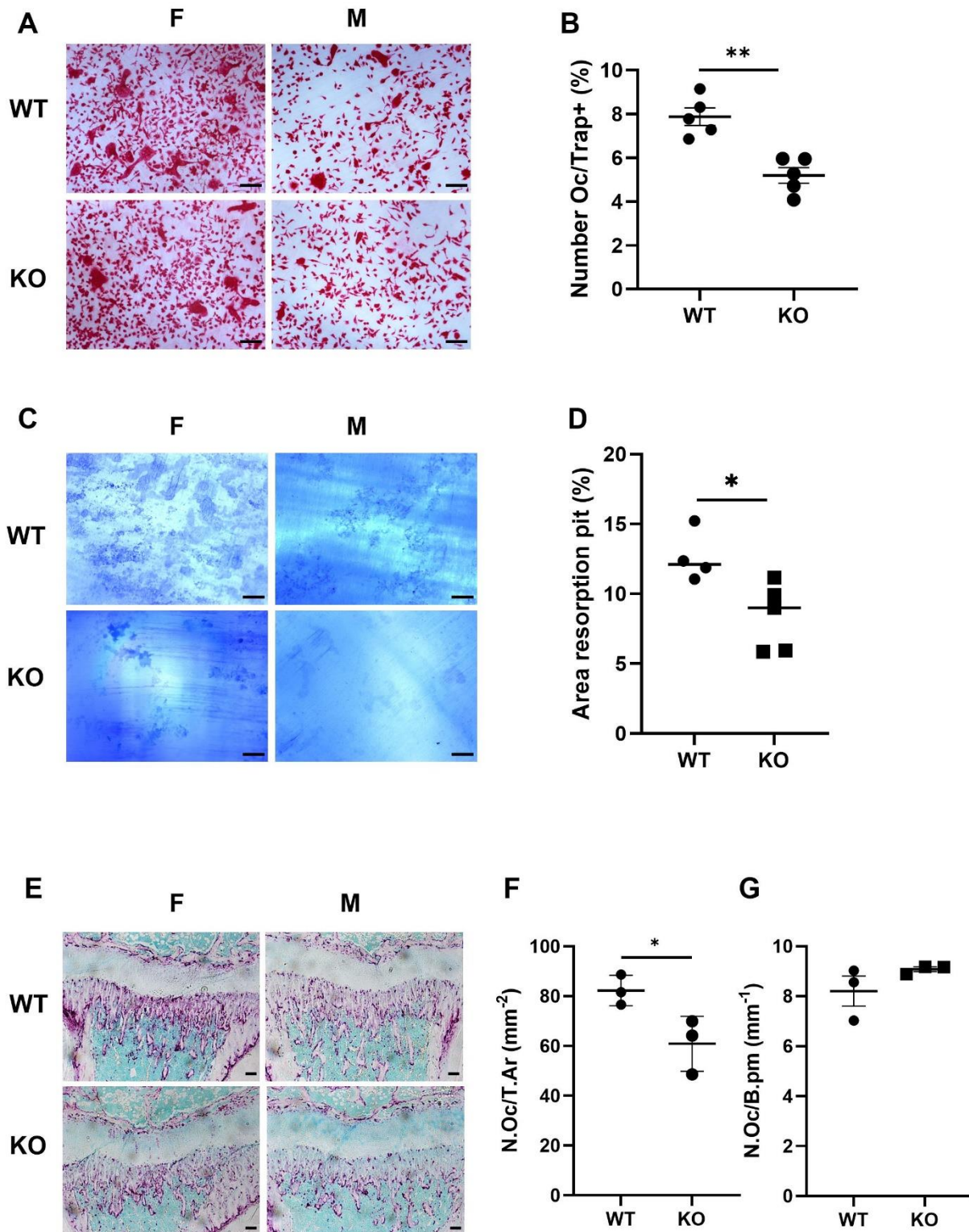


Figure 3: Osteoclastogenesis, osteoclast number and function. A, B.: MCSF-dependent bone marrow macrophages were cultured from the bone marrow of 3-5 weeks old miR-455 null (KO) or wild-type (WT) mice and subjected to an osteoclastogenesis assay with cells cultured on dentine slices. TRAP staining identified and image analysis measured multinucleated osteoclasts (A, B), whilst Toluidine Blue (C, D) staining of dentine showed resorption pits. Mean  $\pm$  SEM,  $n=5$ , Student's t-test, \*,  $p<0.05$ , \*\*,  $p<0.01$ . TRAP staining in the distal tibia of 3 week old mice showed osteoclasts in the primary spongiosa (E), with quantification expressed per unit area (F) or bone volume (G). Scale bar =  $100\mu\text{m}$ .

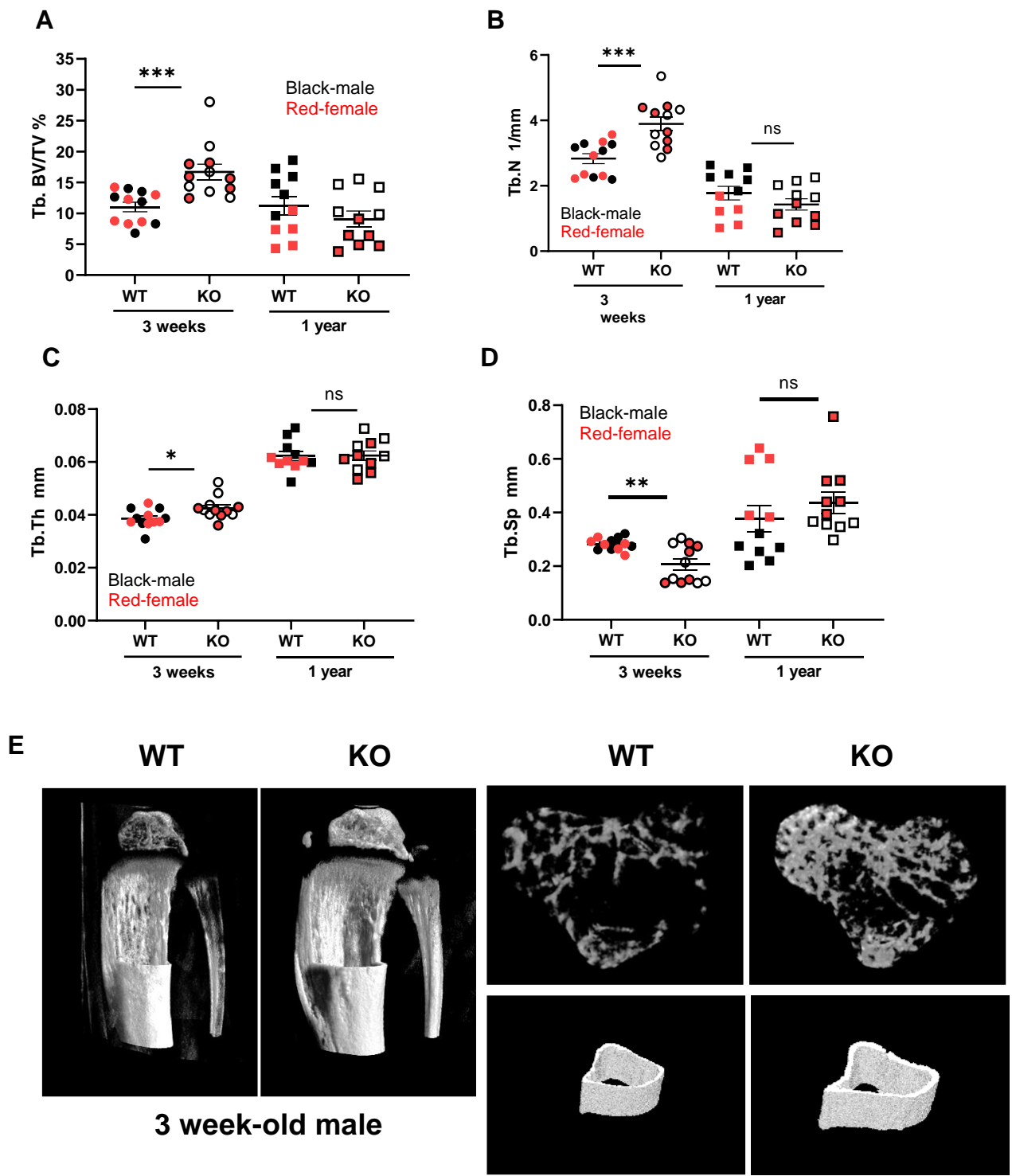


Figure 4: MicroCT analysis of miR-455 null mouse vs. wild-type bone. Mouse hind limbs were dissected, fixed and dehydrated and scanned using a Skyscan 1174 (Bruker), see Methods. A-D: Tb.BV/TV%, percent trabecular bone volume; Tb.N, trabecular number; Tb.Th, trabecular thickness; Tb.Sp, trabecular separation. E, Three dimensional visualization of the tibiae was generated using Ctvol (Bruker).

Gene	Fold miR-455 null vs WT (knee cartilage)	Fold miR-455-3p mimic vs control (SW1353)	Fold miR-455-3p inhibitor vs control (SW1353)	Fold miR-455-3p mimic vs control (chick limb bud)	Predicted target miR-455-3p
<i>Vcan</i>	2.09	0.70	0.98	0.91	N
<i>Alox15</i>	2.80	-	-	-	Y
<i>Penk</i>	2.01	-	-	0.83	N
<i>Srd5a1</i>	2.05	0.88	0.94	0.67	Y
<i>Col2a1</i>	2.03	-	-	1.04	Y
<i>Bmp4</i>	2.76	0.94	1.32	1.15	Y
<i>Bmpr1a</i>	1.42	1.02	0.84	0.87	Y
<i>Epyc</i>	4.27	-	-	1.31	N
<i>Fgf18</i>	2.69	0.56	6.20	0.99	Y
<i>Hjv</i>	3.44	1.68	0.71	0.67	Y
<i>Col9a1</i>	3.09	-	-	0.83	N
<i>Ifitm1</i>	2.07	0.83	0.89	-	N
<i>Panx3</i>	2.34	0.65	0.88	0.86	N

Table 1: Gene expression across RNA-Seq data: Knee articular cartilage taken from 3 month-old miR-455 null mice compared to wild-type; SW1353 cells overexpressing either miR-455-3p mimic or inhibitor vs control (50nM) ; developing chick limb bud was microinjected with miR-455-3p mimic vs control (4µl of 1mM) at HH20-21 and incubated for 24 hours.

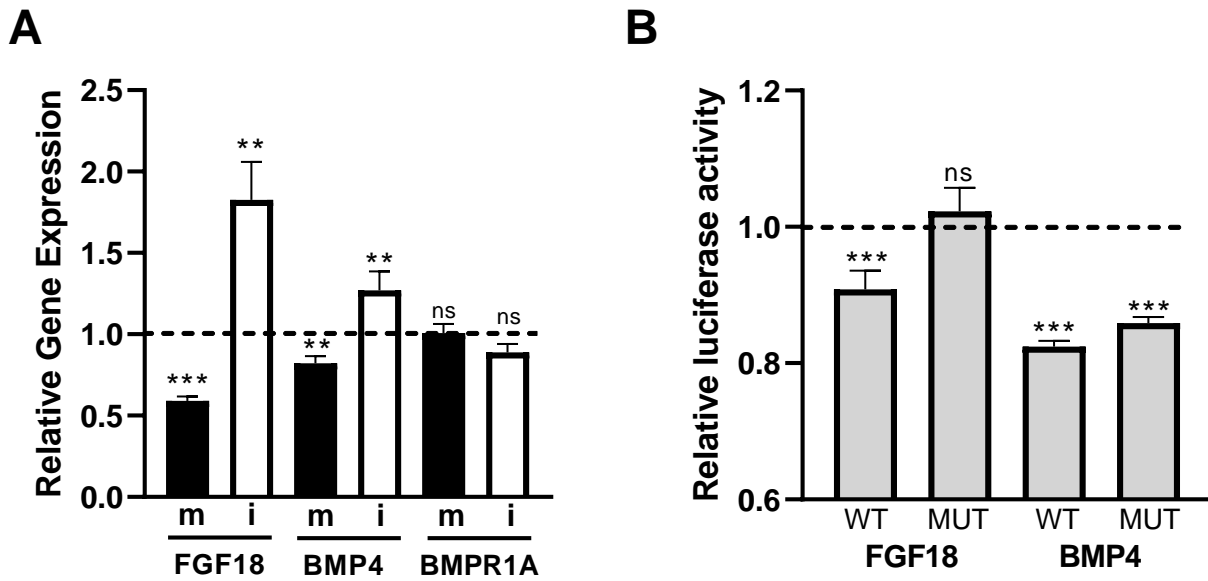


Figure 5: Identification and validation of relevant miR-455 targets. A: Human 143B osteosarcoma cells were transfected with 150 nM miR-455-3p mimic vs control or 75 nM miR-455-3p inhibitor vs control for 48 hr prior to measurement of gene expression by qRT-PCR. Results are expressed as fold expression compared to control (dotted line). B: Chick DF1 fibroblasts were transfected with 100 ng 3'UTR of *FGF18* or *BMP4* in pmiRGLO, either WT sequence or with miR-455-3p targets mutated (mutant) in the presence 50 nM miR-455-3p mimic or non-targeting control for 48 hrs prior to harvest and luciferase assay. Results are plotted relative to non-targeting control (dotted line). Mean +/- SEM, n=4, Student's t-test, \*, p<0.5, \*\*, p<0.01, \*\*\*, p<0.001.

## Supplementary Information

### **Supplementary methods:**

#### Measurement of growth plate

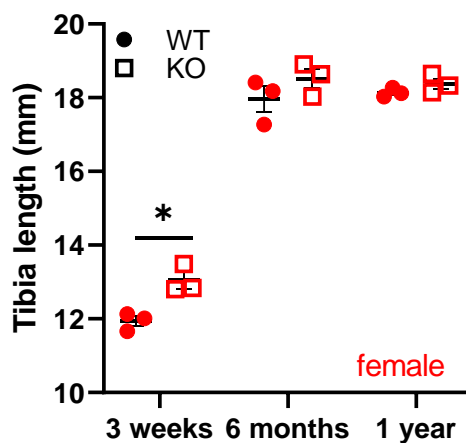
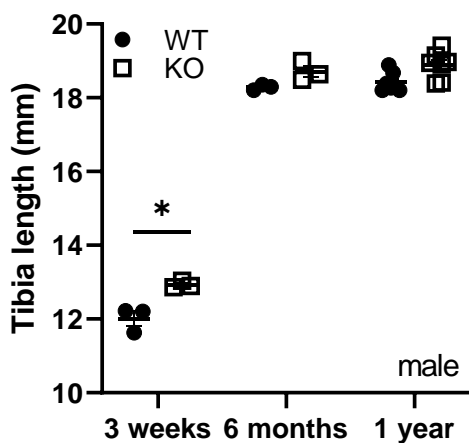
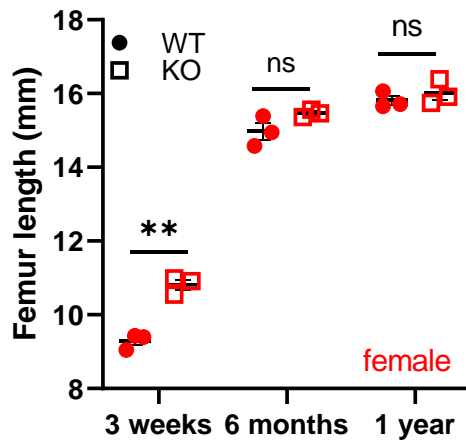
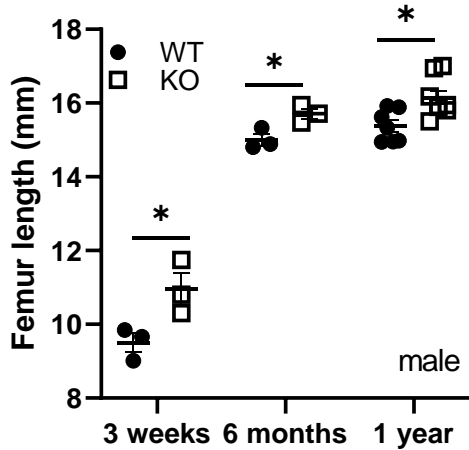
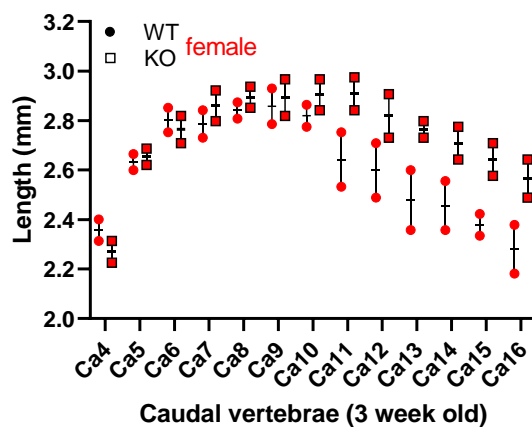
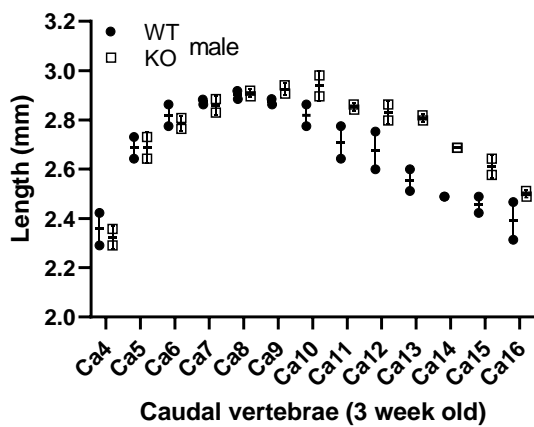
Knee joints were harvested and fixed in 10% (v/v) neutral buffered formalin, followed by decalcification: 14% (w/v) EDTA for one week was used to decalcify 3 week old mice knees. 20% (v/v) formic acid for 24 hours was used to decalcify knees over 6 months old. After decalcification, mice knees were dehydrated in gradient ethanol and embedded in paraffin. Paraffin-embedded tissues were serially sectioned at an interval of 5 $\mu$ m with a thickness of 6 $\mu$ m. Sections were stained with 0.1% (w/v) Safranin O and counterstained with 0.06% (w/v) Fast Green solution. Different zones of the growth plate were defined in terms of cell morphology and staining. The resting zone was defined as the area on top of the growth plate with scattered cells. Beneath the resting zone, the proliferative zone was the region where columns of chondrocytes reside. Hypertrophic zones presented reduced Safranin O staining and enlarged chondrocytes.

#### Staining of adipocyte ghosts

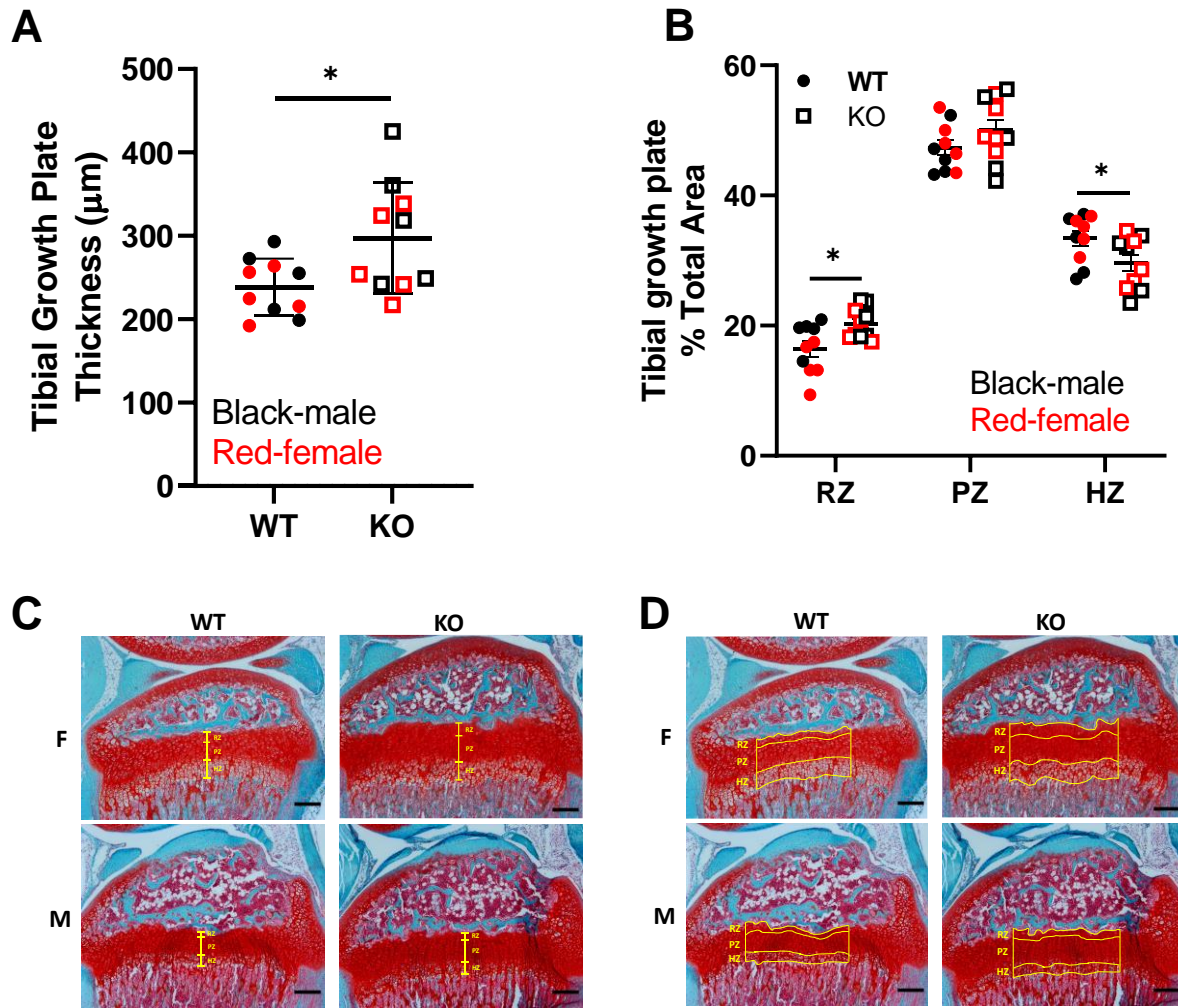
Sections from 3 week old mice were stained with 0.1% (w/v) Safranin O, 0.06% (w/v) Fast Green, following the same method described above. During processing for paraffin embedding, lipids were dissolved, leaving holes in tissues, known as 'adipocyte ghosts'.

#### Destabilisation of the medial meniscus

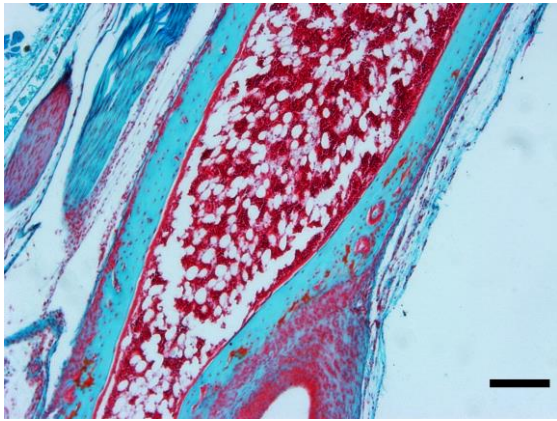
Ten-week-old male mice were anesthetized by inhalation of isoflurane (3% for induction and 1.5–2% for maintenance) in oxygen (1.5–2 liters/minute). All mice received a subcutaneous injection of buprenorphine (Alstoe Animal Health) postsurgery. The mice were fully mobile within 4–5 minutes after withdrawal of isoflurane. DMM was performed as previously described (Glasson et al 2010)), and sham surgery consisted of capsulotomy only OA was scored by 2 individuals in a blinded manner, using a validated histologic scoring system, as described previously (Glasson et al 2010), and results were expressed as the summed score for all four joint components.



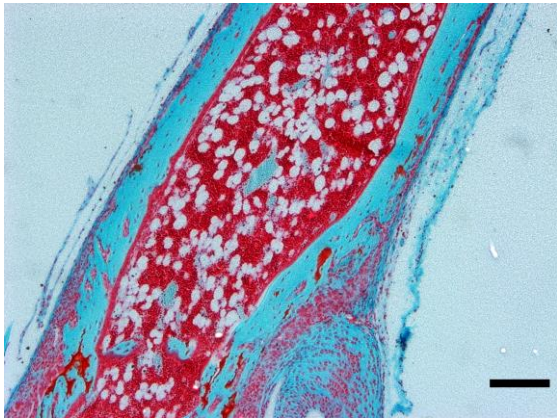
Supplementary Figure 1: Measurement of bone length across age separated by sex A: Caudal (Ca) vertebrae were measured on X-ray and numbered from Ca4 (after lumbar vertebrae), n=2, mean +/- range B, C: Length of tibia and femur were measured on X-ray, n=3-7, t-test with Benjamini-Hochberg correction, \*,  $q < 0.05$ ; \*\*,  $q < 0.01$



Supplementary Figure 2: Tibial growth plate measurement. Coronal sections from 3-week old mice were stained with Safranin O and Fast Green and thickness (A, C) and width (B, D) of resting zone (RZ), proliferative zone (PZ) and hypertrophic zone (HZ) was measured along the growth plate at a similar location using Image J.

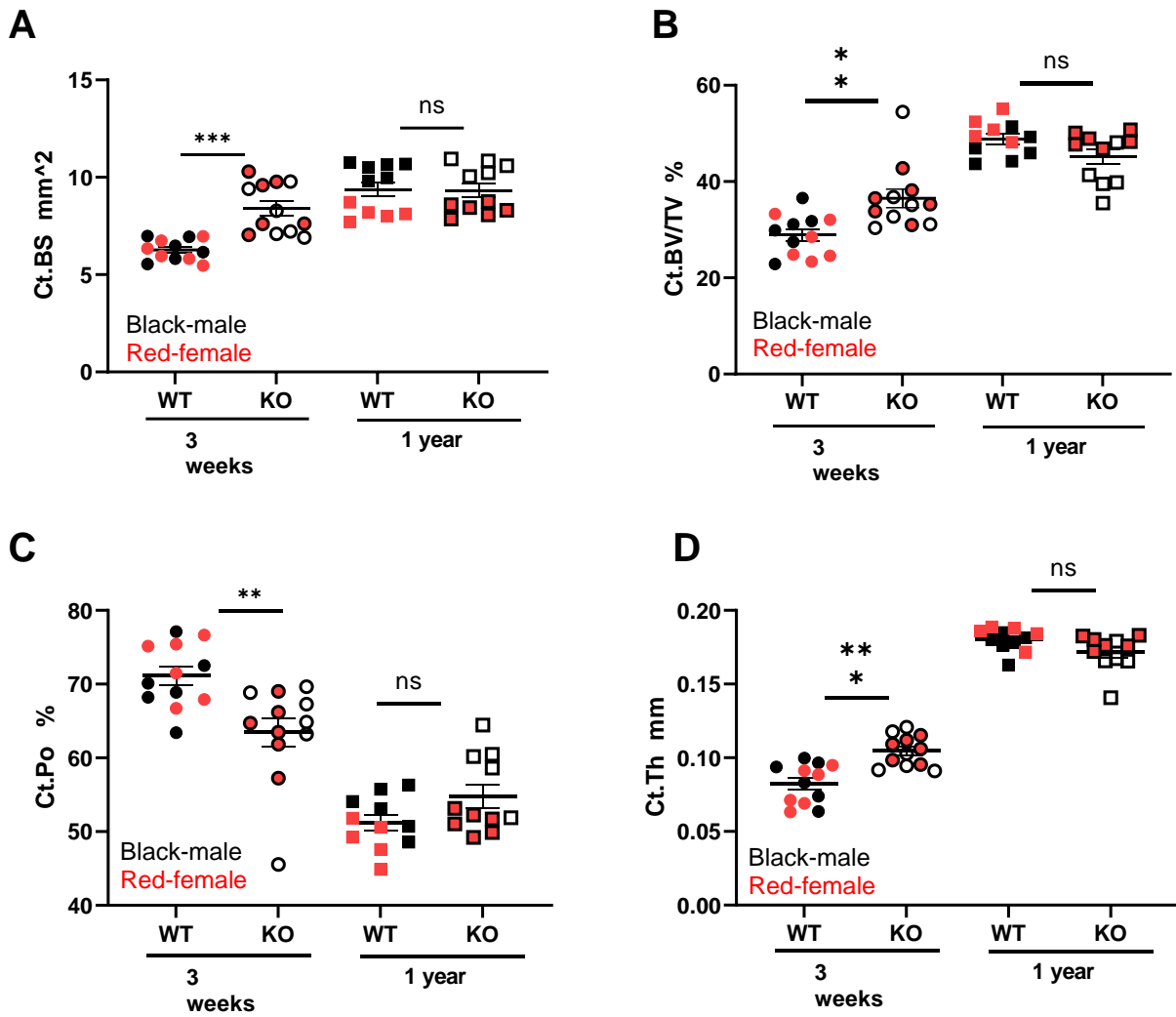


**WT**

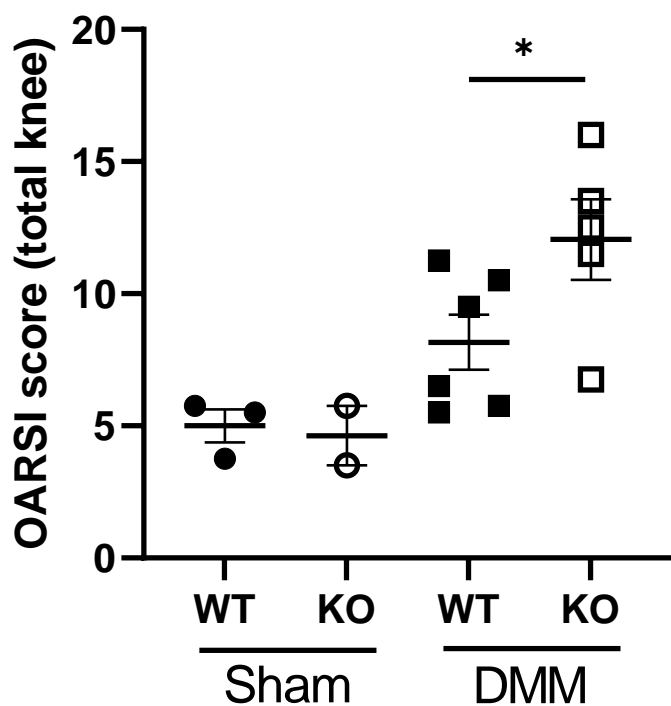


**KO**

Supplementary Figure 3: Adipocyte ghosts within the bone marrow of the distal tibiae of 3-week old mice. Sections were stained with Safranin O and Fast Green. Scale bar = 100 $\mu$ m.



Supplementary Figure 4: MicroCT analysis of miR-455 null mouse vs. wild-type bone. Mouse hind limbs were dissected, fixed and dehydrated and scanned using a Skyscan 1174 (Bruker), see Methods. A-D: Ct.BS, cortical bone surface area; Ct.BV/TV, percent cortical bone volume; Ct.Po, percent cortical porosity; Ct.Th, cortical bone thickness.



Supplementary Figure 5: Destabilisation of the medial meniscus in 12-week old male mice, wild-type (WT) vs. miR-455 knockout (KO), harvested at 10 weeks post-surgery (n=6). Sham surgery knees (n=3) were operated by opening the capsule but without cutting the medial meniscotibial ligament. Osteoarthritis scores, using the OARSI semi-quantitative scoring system (Glasson et al 2010) were assessed by two blinded observers and the summed score for all four joint compartments is shown.

Glasson S, Chambers M, Van Den Berg W, Little C. The OARSI histopathology initiative—recommendations for histological assessments of osteoarthritis in the mouse. *Osteoarthritis and cartilage*. 2010;18:S17-S23

Supplementary Table 1 Primers and UPL (Roche Universal Probe Library) probes for qRT-PCR

Gene	Forward 5'-3'	Reverse 5'-3'	UPL#
<i>BMP4</i>	GGAGGAGGAGGAAGAGCAGA	CACTGGTCCCTGGGATGTTC	31
<i>FGF18</i>	TACCTGTGCATGAACCGCAA	GGCCGTGTAGTTGTTCTCCA	60
<i>BMPR1A</i>	TCAAACGTTTGC GGCCAATT	AATGCTGTGAGTCTGGAGGC	107
<i>VCAN</i>	TGAGGTTGCAACACCACCAT	TTTTGCAGCGATCAGGTCT	97
<i>ALOX15</i>	TCAGGTTCCCTTGTTACCGC	CAGCTCTTCTTCCCGGTGTT	124
<i>SRD5A1</i>	GAGGCAAAGGCATCTGGACT	CACAGGCAGAGCAGCTTACT	23
<i>SFRP2</i>	ACCATTTCTGCTCCGGGATC	AGGAAATGCTGGGGATGCAA	64

Supplementary Table 2 Primers sequences for In-Fusion cloning and site-directed mutagenesis.

3'UTR	Forward-SacI 5'-3'	Reverse-XhoI 5'-3'	Site mutation 5'-3'
<i>BMP4</i>	TTGTTTAAACGAGCTCGAT CAGGCAGTCCTTGA	CGACTCTAGACTCGAGAC CTTTAAATAATGACTCAT TTTAT	CTCACCCACACACTA CACAGACTGCTTCCTT ATAGCT <b>CTCGAG</b> TTAT TTAAAAAAAAAAAAAAAA AAAAGGAAAAAATCC CTA
<i>FGF18</i>	TTGTTTAAACGAGCTCCCA CACTCACACTCCCAGAAA	CGACTCTAGACTCGAGTG TTGAGGCAGTAATACTTG GTT	GATGACAAAAGACTC ACGCAAAG <b>CTCGAG</b> T AGTCAACCCACAGGT GCTTGTC
<i>BMPR1 A</i>	TTGTTTAAACGAGCTCATA TTGGTGGCCGGTGGTTT	CGACTCTAGACTCGAGTG CTTCCACACACCATTTGA	Site 1: GGCCAAAAGAAGTTT AAAGCATCTGTAAATT <b>TCTCGAG</b> TTTTCTTC AACCACCATTTTTTTT GTGG Site 2 and 3: CGCTCTGTGCGCCAG GCT <b>CTCGAGCGAG</b> CT <b>CCAGTGGCGCAATCT</b> CGGC

VCAN	TTGTTTAAACGAGCTCAGC CATAGGTGCAGTTTGCT	GACTCTAGACTCGAGTCTT TGGTCAAACAAAAGCAGA T	Site 1: TAATTTAGTTTGTAGAG CAACTTGAAGAAGAG TAGACAAAAAATAAAA <b>CTCGAG</b> TAGAAAAG AGAAAAGGGCACAA AG Site 2: TGATCTAGTAGGTTTC TATTTTTCCTTTCTCTT TACA <b>CTCGAG</b> TAATA CTTTCCTGTATTTATA TCATAACGTGTATAGT G
SRD5A 1	TTGTTTAAACGAGCTCTAG CCGGGAAAACCTCCGTTC	CGACTCTAGACTCGAGAG CAAAAATTAAGTAGCATCT AA	GGAGTTGAAAACATG TCCACACAGAAAACC <b>TCTCGAG</b> GAATGTTTA TAGCAGCTTTACTCAA AATTGC